

# Quantum phase transition of the Bose-Hubbard model with anisotropic hopping on a cubic lattice

Tao Wang (汪涛) and Xue-Feng Zhang (张学锋)<sup>✉</sup>

*Department of Physics, and Center of Quantum Materials and Devices, Chongqing University, Chongqing 401331, China*



(Received 24 February 2020; revised 17 June 2020; accepted 17 July 2020; published 30 July 2020)

In a quantum many-body system, dimensionality plays a critical role in determining the type of quantum phase transition. To study the quantum system during dimensional crossover, we studied the Bose-Hubbard model on a cubic lattice with anisotropic hopping by using the high-order symbolic strong-coupling expansion method. The analytic series expanded boundaries between the Mott insulator and the superfluid phase up to eighth order are calculated. The critical exponents are extracted by the Padé resummation method, which clearly shows dimensional crossover behavior. Meanwhile, the critical points at commensurate filling can also be obtained, and they match well with the prediction of renormalization group theory. Finally, the scaling of the gap energy and the whole phase diagram are given, and they can be taken as the benchmark for experiment and numerical simulations in future study.

DOI: [10.1103/PhysRevB.102.024522](https://doi.org/10.1103/PhysRevB.102.024522)

## I. INTRODUCTION

Ultracold bosonic atoms trapped in an optical lattice [1], which is described by the Bose-Hubbard model [2,3], are considered a good platform for quantum simulation due to the lattice's flexibility and the fine-tunability of various quantum parameters [4,5]. By interfering three laser beams that are perpendicular to each other with their counterpropagating beams, a three-dimensional (3D) optical lattice can be constructed, and the quantum phase transition (QPT) [6] between the Mott insulator and the superfluid phase can be easily observed with the time of flight by tuning the strength of the laser beams (equivalent to the depth of the lattice potential) [1]. Meanwhile, the system can be realized in different dimensions by varying the strength of the laser beams in different directions [7,8]. According to the Mermin-Wagner theorem [9], the type of phase transition is highly related to the dimensionality. In one dimension, the Mott insulator and the superfluid QPT belong to the Berezinskii-Kosterlitz-Thouless (BKT) universality class, and this results in the reentrance behavior near the tip of the Mott lobe [7,10]. Moreover, the Bose-Hubbard model in higher dimensions ( $d \geq 2$ ) can be solved analytically using the mean-field approach [2], and the QPT is numerically verified to be  $(d + 1)$ D XY universality class [11,12].

The above-mentioned advances have motivated research in the dimensional crossover for ultracold bosons in an optical lattice [7,8,13–21], which can easily be realized experimentally by coupling arrays of 1D bosonic tubes [18]. Based on the mean-field theory, the renormalization-group (RG) approach [13,14], and quantum Monte Carlo (QMC) simulations [17,19], for a 1D to 2D crossover the BKT type QPT only exists in exactly one dimension. This means that infinitesimal intersite tunneling in other directions will cause the transition

to be 3D XY type in the thermodynamic limit [22]. In addition, the changing of critical points at the commensurate filling is numerically demonstrated to be well described by the RG method [13–15,23]. However, it is difficult to numerically study the QPT of a 1D to 3D crossover because of the drawbacks of different numerical approaches [24].

In this paper, we use the high-order symbolic strong-coupling expansion method (HSSCE) [25–27] to study 2D arrays of coupled 1D tubes of ultracold bosonic gas, where the intertube coupling is varied from zero to the same value as the intratube coupling, so that the system can be detuned from 1D to 3D. Based on the process-chain algorithm [26], the strong-coupling expansion [25], and symbolization, the HSSCE can give the symbolic series expansion function of the critical line between the compressible phase (Mott insulator) and the incompressible phase (superfluid) up to very high order for different atom filling numbers and anisotropy (up to eighth order in this work, listed in Appendix A). In previous work [27], we implemented HSSCE to isotropic 1D, 2D, and 3D Bose-Hubbard models, together with a Padé resummation. We obtained very accurate phase boundaries, which are indistinguishable from the numerical results, and we also obtained the critical exponents from the function of a charge gap. Thus, we expect that the HSSCE can also provide highly accurate results from the anisotropic 3D Bose-Hubbard model. These results will not only be beneficial for understanding the QPT during the 1D to 3D crossover, but they can also be used as a benchmark of the experiments and numerical simulations.

This paper is structured as follows. In Sec. II, after briefly introducing the anisotropic 3D Bose-Hubbard model, we describe how to implement the HSSCE in this model, especially dealing with the anisotropy. Then, by listing the eighth-order symbolic results in Appendix A, we discuss the universality class of the phase transition changing during the 1D to 3D crossover in Sec. III, and we give the quantum phase diagram of the Mott insulator to superfluid phase for different filling and anisotropy. Meanwhile, we demonstrate how the tip of

\*Author to whom all correspondence should be addressed:  
zhangxf@cqu.edu.cn

the Mott lobe fulfills the RG prediction for different filling. Finally, we present our conclusions in Sec. IV.

## II. MODEL AND METHOD

The model we considered is the Bose-Hubbard model on a cubic lattice with an anisotropic hopping amplitude:

$$\hat{H} = -t \left( \sum_{\langle i,j \rangle_x} \hat{b}_i^\dagger \hat{b}_j + \alpha \sum_{\langle i,j \rangle_{y,z}} \hat{b}_i^\dagger \hat{b}_j + \text{H.c.} \right) + \frac{U}{2} \sum_i \hat{n}_i (\hat{n}_i - 1) - \mu \sum_i \hat{n}_i, \quad (1)$$

where the hopping amplitude in the  $x$  direction is  $t$ , and those in the  $y, z$  directions are  $\alpha t$  with the anisotropic parameter  $0 \leq \alpha \leq 1$ ;  $\hat{b}_i^\dagger$  ( $\hat{b}_i$ ) is the creation (annihilation) operator on site  $i$ ;  $\hat{n}_i$  is the local density operator;  $U$  is the on-site two-body interaction, which can be detuned with Feshbach resonance; and  $\mu$  is the chemical potential. When  $\alpha$  is equal to 1, the system is isotropic in three dimensions, while in another limit,  $\alpha = 0$ , all the hoppings in the  $y$  and  $z$  directions are shut off, and the 2D array of Bose-Hubbard chains is decoupled, so that the system can be treated as 1D. In both limits, there exist the QPTs between the Mott insulator and the superfluid phase. The upper (lower) phase boundary of the Mott lobe is caused by particle (hole) excitation, and the dynamical exponent is  $z = 2$ , while at the tip of the lobe the effective particle-hole symmetry leads to  $z = 1$  [2]. All the phase diagrams can be obtained with a degenerate perturbation theory called the strong-coupling expansion method [25].

Taking the hopping matrix as the perturbative term, the strong-coupling expansion method aims to calculate the energies of the ground state and single-particle (hole) excited state in the Mott insulator. Then, the series expansion function of the upper (lower) phase boundary can be obtained by comparing the ground-state energy with the single-particle (hole) excited one. However, because of the exponential increment of the calculation for higher orders, high precision cannot be achieved.

In the process chain approach [26], the Kato representations can be used to diagram the perturbative contributions in each order. After simplifying the diagrams by considering the different symmetries (e.g., point symmetry) and topology, the number of diagrams can be significantly decreased. Then, we can achieve very high order (e.g., 10th order [27]) by numerically computing each diagram. Meanwhile, the whole process is symbolized in our previous work [27] so that the results can be considered as an exact Taylor expansion of the phase boundaries, thus it can provide a more accurate analysis of the QPT. Because the computational resource consumption is more sensitive to the orders than the dimensionality, the HSSCE is very suitable for quantitatively studying the QPT during the dimensional crossover.

The algorithm and source code of the HSSCE were given in Ref. [27]. Extending the HSSCE to an anisotropic system is pretty straightforward, with the difference being a simplification of the diagrams. Due to the anisotropy of the system, the point symmetry is lower than before, so the numbers of the equivalent diagrams are less than before. Thus, the calculation

requires more computing hours than in the isotropic case. After comparing the perturbative energy of the ground state and the single-particle (hole) excited state, we obtain the upper and lower boundaries:

$$\begin{aligned} \text{particle: } \frac{\mu_p}{U} &= n - \sum_k \beta_u^{(k)}(\alpha, n) \left( \frac{t}{U} \right)^k, \\ \text{hole: } \frac{\mu_h}{U} &= n - 1 + \sum_k \beta_d^{(k)}(\alpha, n) \left( \frac{t}{U} \right)^k, \end{aligned} \quad (2)$$

where the coefficients of the boundaries are  $\beta_{u(d)}^{(k)}(\alpha, n) = \sum_{i=1}^{k+1} \sum_{j=1}^{k+1} \alpha^{i-1} B_{i,j}^{u(d)}(k) n^{j-1}$  with the coefficient matrix  $B_{i,j}^{u(d)}(k)$ , which can be symbolically output by the HSSCE and is listed in Appendix A up to eighth order.

## III. RESULTS

The HSSCE is a symbolic algorithm, as presented in Eq. (2) and Appendix A. The results can be considered as the analytic Taylor expansion of boundaries for all the parameters. However, the boundaries have singularities at the tip of the Mott lobe. This means that only the phase transition in the strongly coupled region  $t/U \ll 1$  can be well described by the raw data, but not around the singularities. However, as the most important part of the QPT, the universality class can be well detected by checking the scaling behavior of the gap energy  $\Delta = \mu_p - \mu_h$  with respect to the quantum parameter  $t/U$  around the tip of the lobe. Thanks to the Padé resummation method, the behavior of the singularity can reappear. In one dimension, the reentrance behavior demonstrates the BKT universality class, and the critical exponents  $z\nu$  can be obtained for higher dimension, in which the phase transition belongs to the  $(d+1)$ D XY universality class [27].

For the anisotropic system at finite temperature, there is a dimensional phase transition from the 1D Luttinger liquid to the 3D Bose liquid [8]. In comparison, at zero temperature, condensation can exist for an arbitrarily small anisotropic parameter  $\alpha$ , so the QPT for the 1D to 3D crossover region should be belong to 4D XY type except for the pure 1D point  $\alpha = 0$ , which belongs to BKT type [22].

In the thermodynamic limit, the charge gap of the Bose-Hubbard model in  $d \geq 2$  dimensions follows the power-law scaling  $\Delta = A(t)(t_c - t)^{z\nu}$  [2], where  $A(t)$  is a regular function and  $z, \nu$  denotes the critical exponents that characterize the scaling of long-range correlation. Thus, the logarithm of the charge gap

$$\frac{\partial \ln \Delta}{\partial t} = \frac{A'(t)}{A(t)} + \frac{z\nu}{t_c - t} \quad (3)$$

has a simple pole  $t_c$  and could be determined by the Padé resummation method:

$$\frac{\partial \ln \Delta}{\partial t} = \frac{\sum_{n=0}^{n_{\max}} a_n t^n}{1 + \sum_{m=0}^{m_{\max}} b_m t^m}. \quad (4)$$

The coefficients  $a_n$  and  $b_m$  could be calculated by fitting with the restriction  $n_{\max} + m_{\max} = 8$ . Here we choose the most natural way, i.e.,  $n_{\max} = m_{\max} = 4$  (other possible choices are discussed in Appendix B). The smallest real positive simple

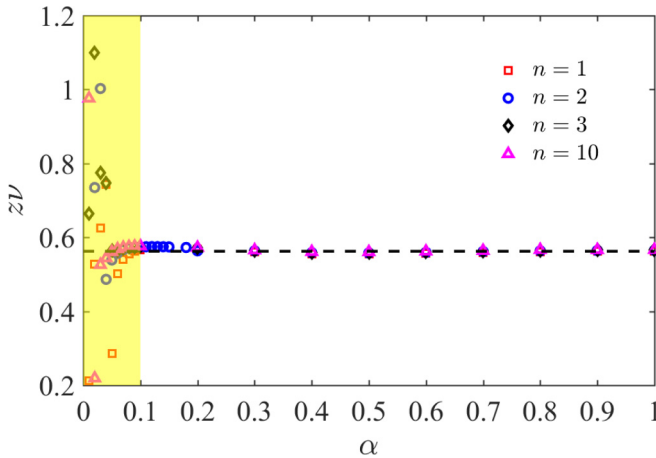


FIG. 1. The critical exponents  $z\nu$  changing with  $\alpha$  for different filling number  $n$ . For most of the region, the values of  $z\nu$  are approximately around 0.56 (black dashed line) and less sensitive to the anisotropy  $\alpha$  and filling number  $n$ . However, when  $\alpha \lesssim 0.1$  (yellow region), the critical exponents  $z\nu$  become messy.

pole gives the critical hopping amplitude  $t_c$  at the lobe tip or commensurate fillings, while the corresponding residue yields the critical exponent  $z\nu$ .

We show the critical exponents  $z\nu$  for different filling and anisotropy in Fig. 1. When  $\alpha \gtrsim 0.1$ , the results demonstrate that the phase transitions are of a 4D XY type universality class with critical exponents the same as in the isotropic 3D case  $z\nu \approx 0.5625$ . Because  $d+1=4$  is the upper critical dimension of the XY model, the logarithm correction may result in a discrepancy with the mean-field value  $z\nu = 1/2$ . However, when approaching the 1D limit, the fitting of critical exponents starts to be invalid. Such phenomena are not related to the filling numbers, and we think they result from the limitation of perturbative orders. As shown in Appendix A, for each perturbative term, each element of the coefficient matrix is also series-expanded with respect to  $\alpha$ . Thus, when  $\alpha$  is less than 0.1, the high power order of  $\alpha$  will contribute less, which means the result is more like the 1D case. To make the 4D XY type fitting still work for strong anisotropy, higher-order terms are necessary.

In one dimension, the Bose-Hubbard chain undergoes the BKT QPT, and the charge gap fulfills exponential scaling behavior  $\Delta = B(t) \exp(-\frac{W}{\sqrt{t_c-t}})$ , where  $B(t)$  is a regular function,  $W$  is the fitting parameter, and  $t_c$  is the critical point, which could also be captured by Padé resummation of  $[\ln \Delta(t)]^2$ . Different from the 4D-XY type fitting, the smallest real positive pole is taken after canceling out the common zero points of the denominator and numerator. As shown in the inset of Fig. 2, when  $\alpha = 0.05$ , which is smaller than the critical value 0.1, the charge gap function with 4D XY-type fitting exhibits a rounded tip that is very different from the sharp shape in a one-dimensional system. To depict the whole anisotropy region in a proper way, as shown in Fig. 2, we adopt a 4D XY-type and a BKT-type fitting for  $\alpha \geq 0.1$  and  $\alpha < 0.1$ , respectively. We can find the charge gap function changing from rounded to sharp with decreasing  $\alpha$ , and it demonstrates the scaling behavior changing during the di-

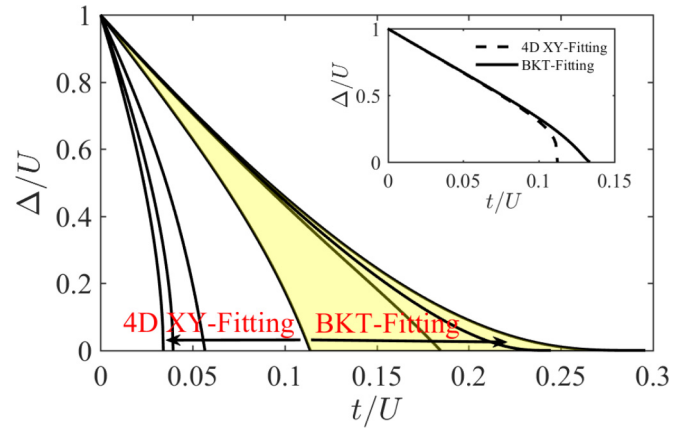


FIG. 2. The charge gap function with different  $\alpha$  (right to left: 0, 0.005, 0.01, 0.1, 0.5, 0.8, and 1) for  $n = 1$ . For  $\alpha \geq 0.1$ , the 4D XY type fitting  $A(t)(t_c - t)^{z\nu}$  is adopted, while for  $\alpha < 0.1$ , the BKT type fitting  $B(t) \exp(-\frac{W}{\sqrt{t_c-t}})$  is chosen. Inset: two types of fitting at  $\alpha = 0.05$  and  $n = 1$ .

mensional crossover. If higher-order terms can be considered in future work, we think the deep anisotropic region can be approached with 4D XY-type fitting. Considering the high accuracy of the HSSCE, our results on the charge gap function can be taken as a benchmark for numerical simulations [10–12] and experiments [1,7].

The anisotropic 3D system can be treated as a 2D array of a coupled 1D tube. Because the one-dimensional Bose-Hubbard model can be well described by the bosonization [28], the dimensional crossover problem can be solved analytically with help from the RG approach [13,14,23,29]. After taking couplings in  $y(z)$  directions as the perturbation of the effective bosonized 1D Hamiltonian, the RG equations can be constructed [7,8,13,14,19,23] as follows:

$$\frac{dg_J}{dl} = \left(2 - \frac{1}{2K}\right)g_J, \quad (5)$$

$$\frac{dg_u}{dl} = (2 - K)g_u, \quad (6)$$

$$\frac{dK}{dl} = 4g_J^2 - g_u^2 K^2, \quad (7)$$

where  $g_J$  and  $g_u$  are dimensionless parameters characterizing the strength of hopping in the  $y$  ( $z$ ) direction and the periodical “Mott potential,”  $K$  is the Luttinger parameter of a 1D Bose-Hubbard chain, and  $l$  is the flow parameter. After comparing with the RG equations of the 1D to 2D crossover [19], we find that the only difference is that the coefficient of the first term in  $dK/dl$  is 4, not 2. Because the RG analysis is around  $K(l) \approx 2$ , and  $g_J$  is set to be zero, the analytical relation between anisotropy  $\alpha$  and critical point  $t_c(\alpha)$  for the superfluid to Mott-insulator transition at commensurate fillings is the same:

$$\alpha = C \exp\left(-\frac{\pi s}{4b\sqrt{t_c^{1D}/t_c(\alpha) - 1}}\right), \quad (8)$$

where  $C$  and  $b$  are constants,  $t_c^{1D}$  is the critical hopping amplitude of the lobe tip for the 1D Bose-Hubbard model,

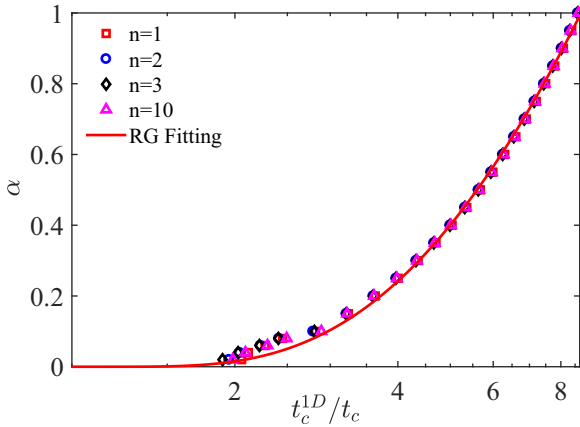


FIG. 3. The relation between critical hopping amplitude  $t_c$  at commensurate fillings and the anisotropic parameter  $\alpha$ . The discrete data point are obtained from Padé resummation Eq. (4) for different filling numbers. The red line is the theoretical fitting based on Eq. (8).

while  $s$  is the constant related to the scaling of the order parameter. Because the charge gap  $\Delta \propto 1/\xi$ , where  $\xi$  stands for the correlation length, here the constant  $s$  is set to be 1. Noting that, different from Ref. [19], we set  $U = 1$  as the energy unit.

As shown in Fig. 3, similar to the 1D to 2D crossover [19], the HSSCE data of critical points at the tips of Mott lobes for different filling numbers nearly coincide with the fitting curve with Eq. (8) except for the small deviations when  $\alpha$  is small. The reason for these deviations is that we use BKT-type fitting for small  $\alpha$ , which is not consistent with the 4D XY-type universality class concluded by RG theory. Such a mismatch can be recovered by including higher order in the future work. The values of constants  $C$  and  $b$  are listed in Table I, and they are less relevant to the filling number. Furthermore, we find that the fitting parameter  $b$  is very close to the 1D to 2D crossover from QMC simulation [19].

Finally, we discuss the whole phase diagram at incommensurate fillings presented in Fig. 4. Because the HSSCE method gives the series expansion results of upper and lower boundaries, the phase diagrams in the grand-canonical ensemble are explicitly provided. As discussed in our previous paper [27], in three dimensions, all coefficients in different orders are positive, so that there is no exotic behavior observed in the phase diagram. In comparison, in a one-dimensional system, some of the coefficients are changed to negative, so that three critical points could exist at the same chemical potential energy  $\mu/U$ , which is called reentrance behavior. Such exotic phenomena are due to the exponential decay of the gap energy, and they also reflect the fact that the QPT belongs to the BKT universality class. In Fig. 4, the phase

TABLE I. The fitting constants for different filling numbers based on Eq. (8).

Constants	$n = 1$	$n = 2$	$n = 3$	$n = 10$
$C$	10.536	10.460	10.455	10.482
$b$	0.120	0.121	0.121	0.120

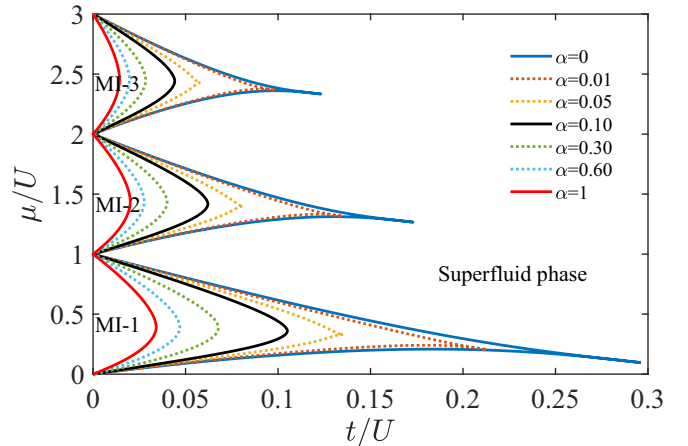


FIG. 4. The whole phase diagram of the anisotropic Bose-Hubbard model for different anisotropy  $\alpha$  (right to left: 0, 0.01, 0.05, 0.10, 0.30, 0.60, 1.00) and different fillings.

boundaries are changing from a rounded shape to a sharp one. Meanwhile, the reentrance can also be found for small  $\alpha$ , which reflects that the dimensional crossover becomes serious when approaching one dimension.

#### IV. CONCLUSION AND DISCUSSION

Taking advantage of the HSSCE method, we get the symbolic series expanded phase boundaries between the Mott insulator and the superfluid phase for the anisotropic Bose-Hubbard model on a cubic lattice up to eighth order. With the Padé resummation method, the related critical exponents  $z\nu$  can be extracted. However, when anisotropy is strong,  $\alpha < 0.1$ ,  $z\nu$  changes drastically. To restore the physical process, we reconstruct the phase boundaries by choosing a 4D XY type fitting for  $\alpha \geq 0.1$ , and a BKT type fitting for  $\alpha < 0.1$ . Then, we study the relation between the critical point at commensurate filling and the anisotropy, and we find that it agrees well with the prediction given by RG theory. Finally, we also give the whole phase diagram at incommensurate filling for different anisotropy  $\alpha$ .

Because of the high flexibility and tunability, the results presented in this work could be checked by cold atom gas experiments in an optical lattice. One could prepare 1D boson gases trapped in a 2D optical lattice [8], thus the hopping amplitude between tubes could be tuned by the intensity of laser coupling in the tubes. The phase transition

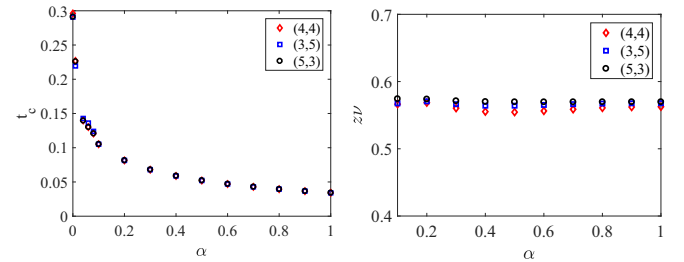


FIG. 5. The critical hoppings and exponents for different Padé degrees at the same commensurate filling.

between superfluid and a Mott insulator could be captured by time-of-flight technology. The location of the tip lobe as a function of the anisotropic parameter could be obtained by detecting the point where plateaus begin from the expansion experiment [18]. In addition, when the trapping potential is introduced, the system will exhibit pancake structures. The phase boundaries can be extracted from the region of each Mott plateau, and they can be compared with our results [30].

## ACKNOWLEDGMENTS

We are thankful for useful discussions with Axel Pelster, Sebastian Eggert, Hong-Hao Tu, and Long Liang. X.-F.Z. acknowledges funding from the National Science Foundation of China under Grants No. 11804034, No. 11874094, and No. 11947406, and Grant No. csc2018jcyJAX0399 by Chongqing Natural Science Foundation. T.W. acknowledges funding from China Postdoctoral Science Foundation funded Project 2020M673118.

## APPENDIX A: THE SYMBOLIC SERIES EXPANSION OF THE PHASE BOUNDARIES FOR THE ANISOTROPIC BOSE-HUBBARD MODEL

The boundaries of the Mott lobe can be represented in series-expansion form:

$$\begin{aligned} \text{particle: } \frac{\mu_p}{U} &= n - \sum_k \beta_u^{(k)}(\alpha, n) \left( \frac{t}{U} \right)^k, \\ \text{hole: } \frac{\mu_h}{U} &= n - 1 + \sum_k \beta_d^{(k)}(\alpha, n) \left( \frac{t}{U} \right)^k, \end{aligned} \quad (\text{A1})$$

where the coefficient of the upper boundary is  $\beta_u^{(k)}(\alpha, n) = \sum_{i=1}^{k+1} \sum_{j=1}^{k+1} \alpha^{i-1} B_{i,j}^u(k) n^{j-1}$ , and the coefficient matrixes  $B_{i,j}^u(k)$  are

$$\begin{aligned} \mathbf{B}^u(1) &= \begin{pmatrix} -4 & -4 \\ -2 & -2 \end{pmatrix}, \quad \mathbf{B}^u(2) = \begin{pmatrix} 0 & -8 & -6 \\ 0 & -16 & -16 \\ 0 & 0 & 1 \end{pmatrix}, \quad \mathbf{B}^u(3) = \begin{pmatrix} 0 & -16 & -60 & -44 \\ 0 & -68 & -210 & -142 \\ 0 & -20 & -66 & -46 \\ 0 & 2 & 3 & 1 \end{pmatrix}, \\ \mathbf{B}^u(4) &= \begin{pmatrix} 0 & -\frac{135}{2} & -\frac{17857}{60} & -\frac{2449}{6} & -\frac{10597}{60} \\ 0 & -316 & -1838 & -3036 & -1514 \\ 0 & -\frac{622}{3} & -\frac{15659}{15} & -\frac{4766}{3} & -\frac{11239}{15} \\ 0 & -\frac{92}{3} & -\frac{542}{3} & -\frac{892}{3} & -\frac{442}{3} \\ 0 & -\frac{9}{4} & -\frac{559}{120} & -\frac{7}{12} & \frac{221}{120} \end{pmatrix}, \\ \mathbf{B}^u(5) &= \begin{pmatrix} 0 & \frac{31}{3} & -\frac{387253}{450} & -\frac{1638443}{450} & -\frac{2188403}{450} & -\frac{941863}{450} \\ 0 & -\frac{4051}{4} & -\frac{19097321}{1800} & -\frac{58121101}{1800} & -\frac{68366371}{1800} & -\frac{27519641}{1800} \\ 0 & -903 & -\frac{4684909}{450} & -\frac{14775229}{450} & -\frac{17720459}{450} & -\frac{7223789}{450} \\ 0 & -\frac{2522}{9} & -\frac{260017}{75} & -\frac{2510981}{225} & -\frac{1013317}{75} & -\frac{1245971}{225} \\ 0 & -\frac{209}{36} & -\frac{401707}{1800} & -\frac{1456567}{1800} & -\frac{1803257}{1800} & -\frac{737947}{1800} \\ 0 & \frac{653}{72} & \frac{114703}{3600} & \frac{42481}{1200} & \frac{56453}{3600} & \frac{11063}{3600} \end{pmatrix}, \\ \mathbf{B}^u(6) &= \begin{pmatrix} 0 & -\frac{6344897}{6048} & -\frac{12245886137}{1512000} & -\frac{695777273}{25200} & -\frac{70292096771}{1512000} & -\frac{5679281509}{151200} & -\frac{4396126631}{378000} \\ 0 & -\frac{510985}{108} & -\frac{3957402269}{63000} & -\frac{26732808157}{94500} & -\frac{26397560641}{47250} & -\frac{3942882856}{7875} & -\frac{31526579237}{189000} \\ 0 & -\frac{1597247}{216} & -\frac{13883931061}{162000} & -\frac{38573963749}{108000} & -\frac{434792528659}{648000} & -\frac{62651400559}{108000} & -\frac{24361535093}{129600} \\ 0 & -\frac{1029677}{252} & -\frac{1136383799}{21000} & -\frac{92334825139}{378000} & -\frac{40602475367}{84000} & -\frac{23428854167}{54000} & -\frac{36476848183}{252000} \\ 0 & -\frac{897971}{756} & -\frac{6445354697}{567000} & -\frac{10942072933}{252000} & -\frac{50536206163}{648000} & -\frac{49639768249}{756000} & -\frac{3794314171}{181440} \\ 0 & -\frac{4663}{54} & -\frac{53282041}{94500} & -\frac{98446741}{47250} & -\frac{186941341}{47250} & -\frac{9228077}{2625} & -\frac{12233309}{10500} \\ 0 & -\frac{329201}{12096} & -\frac{6145973}{51840} & -\frac{1299931}{7000} & -\frac{1019369927}{9072000} & -\frac{26507951}{1512000} & -\frac{2100869}{4536000} \end{pmatrix}, \end{aligned}$$

$\mathbf{B}^u(7) =$	$\begin{pmatrix} 0 & \frac{17208115}{5292} & \frac{29226199817}{8505000} & \frac{40776313677359}{476280000} & \frac{2860644143681}{7620480} & \frac{17569043110187}{27216000} \\ 0 & \frac{2820543409}{254016} & \frac{261543252131069}{952560000} & \frac{18123177499069}{9720000} & \frac{10677162089359543}{1905120000} & \frac{16028030330232943}{1905120000} \\ 0 & \frac{541247299}{47628} & \frac{7661308452911}{17860500} & \frac{182365471982893}{57153600} & \frac{28505938773306611}{2857680000} & \frac{43743064347892991}{2857680000} \\ 0 & \frac{832739197}{54432} & \frac{586905879598571}{1428840000} & \frac{8185350354028231}{2857680000} & \frac{7126876800312161}{816480000} & \frac{75531105849692267}{5715360000} \\ 0 & \frac{642757627}{190512} & \frac{93304063975439}{714420000} & \frac{21387397577611}{22325625} & \frac{4232810624737243}{1428840000} & \frac{6444199749517843}{1428840000} \\ 0 & \frac{488721839}{381024} & \frac{222894050851}{40824000} & \frac{10436593904551}{114307200} & \frac{1909402585897307}{5715360000} & \frac{63304570520783}{116640000} \\ 0 & \frac{202502513}{762048} & \frac{2243122165069}{2857680000} & \frac{194179244813}{178605000} & \frac{47163130806559}{5715360000} & \frac{83609709293119}{5715360000} \\ 0 & \frac{137725031}{1524096} & \frac{2608966642123}{5715360000} & \frac{2599569516137}{2857680000} & \frac{10042635987533}{11430720000} & \frac{4617015079493}{11430720000} \end{pmatrix} \cdot \dots \cdot \begin{pmatrix} \frac{482685930471859}{952560000} & \frac{20517348363031}{136080000} \\ \frac{2354998048684739}{381024000} & \frac{3373911641427409}{1905120000} \\ \frac{4656897396054443}{408240000} & \frac{9436217113175831}{2857680000} \\ \frac{55815885881231213}{5715360000} & \frac{3212480565675379}{1143072000} \\ \dots \dots & \dots \dots \\ \frac{136403063466893}{40824000} & \frac{1375712097341929}{1428840000} \\ \frac{2369567032887617}{5715360000} & \frac{99107423249021}{816480000} \\ \frac{64070255378107}{5715360000} & \frac{18442465574893}{5715360000} \\ \frac{852816554717}{11430720000} & \frac{13030989991}{2286144000} \end{pmatrix},$
$\mathbf{B}^u(8) =$	$\begin{pmatrix} 0 & \frac{872897054659901}{27461161728} & \frac{18588146435171828297}{70025962406400} & \frac{413569750046670214409}{350129812032000} & \frac{14787600350917688774251}{4376622650400000} \\ 0 & \frac{95005249454097}{114421057020} & \frac{13244337545102475247}{8581613040000} & \frac{264367876414238436491}{21454032600000} & \frac{301580561206259400151}{6129723600000} \\ 0 & \frac{16238352579201839}{68652904320} & \frac{2373252477645589592807}{625231807200000} & \frac{96025127809245373230077}{3501298120320000} & \frac{278085466866232929313049}{2693306246400000} \\ 0 & \frac{13143770575741441}{68652904320} & \frac{995937783105265674239}{257448391200000} & \frac{2350421651369022799319}{73556683200000} & \frac{5331785324269380365833}{41191742592000} \\ 0 & \frac{944433487400923}{68652904320} & \frac{558926136337582161637}{257448391200000} & \frac{158923954308124670199}{102979356480000} & \frac{59148943373367455404739}{1029793564800000} \\ 0 & \frac{507339953516177}{13730580864} & \frac{136657625883731073467}{257448391200000} & \frac{1996276255302159037997}{514896782400000} & \frac{1416193691744932910423}{93617596800000} \\ 0 & \frac{11678789233897}{980755776} & \frac{45265835304985762657}{437662265040000} & \frac{166676575235287627447}{3501298120320000} & \frac{48614865808330901615719}{35012981203200000} \\ 0 & \frac{53092182089}{39007332} & \frac{21947335344624203}{2925549900000} & \frac{454524239184255743}{23404399200000} & \frac{338045490925866803}{9361759680000} \\ 0 & \frac{1666893622223}{4992938496} & \frac{3476906811387841513}{17506490601600000} & \frac{16813066682918948423}{3501298120320000} & \frac{1295331946972830623}{218831132520000} \end{pmatrix} \cdot \dots \cdot \begin{pmatrix} \frac{26671980610761545640463}{4376622650400000} & \frac{10410924449492715109187}{1591499145600000} & \frac{33111769841940340290731}{8753245300800000} & \frac{15828728653296464701673}{17506490601600000} \\ \frac{45624619074402203133}{4290806520000} & \frac{217327134904346719957}{1716322608000} & \frac{1677198534587955706049}{21454032600000} & \frac{838693437524617003943}{42908065200000} \\ \frac{47035289606202568606931}{218831132520000} & \frac{1745666266438961774155609}{7002596240640000} & \frac{105629267865011237851279}{700259624064000} & \frac{12992963132226023742719}{3501298120320000} \\ \frac{181323248371926588827}{6436209780000} & \frac{346809455737849275209449}{1029793564800000} & \frac{107297330482079718457187}{514896782400000} & \frac{53727086003957287993}{102979356480000} \\ \dots \dots & \dots \dots & \dots \dots & \dots \dots \\ \frac{6109681701556168557649}{51489678240000} & \frac{2877194638779880164413}{21016195200000} & \frac{8498901170351000106563}{102979356480000} & \frac{5212373807745931214239}{257448391200000} \\ \frac{4190072201435347478723}{128724195600000} & \frac{39941538353675711318161}{1029793564800000} & \frac{2470393487607124610383}{102979356480000} & \frac{2810981946672182633}{4680879840000} \\ \frac{2215687272058418767953}{8753245300800000} & \frac{27368037637614980966983}{1000370891520000} & \frac{27906138178108288734971}{17506490601600000} & \frac{3363780527662396586096}{8753245300800000} \\ \frac{1282549052137542647}{23404399200000} & \frac{682401984740784199}{11702199600000} & \frac{410522570657836837}{11702199600000} & \frac{58422103525040867}{6686971200000} \\ \frac{4814954013850918313}{1250463614000000} & \frac{434243819219943077927}{35012981203200000} & \frac{288903335083336057}{17506490601600000} & \frac{200810348470291303}{35012981203200000} \end{pmatrix},$

and the coefficient of lower boundary is  $\beta_d^{(k)}(\alpha, n) = \sum_{i=1}^{k+1} \sum_{j=1}^{k+1} \alpha^{i-1} B_{i,j}^d(k) n^{j-1}$ , where the coefficient matrixes  $B_{i,j}^d(k)$  are

$$\mathbf{B}^d(1) = \begin{pmatrix} 0 & 4 \\ 0 & 2 \end{pmatrix}, \quad \mathbf{B}^d(2) = \begin{pmatrix} -2 & 4 & 6 \\ 0 & 16 & 16 \\ -1 & -2 & -1 \end{pmatrix}, \quad \mathbf{B}^d(3) = \begin{pmatrix} 0 & 28 & 72 & 44 \\ 0 & 74 & 216 & 142 \\ 0 & 26 & 72 & 46 \\ 0 & 1 & 0 & -1 \end{pmatrix},$$

$$\mathbf{B}^d(4) = \begin{pmatrix} -\frac{43}{30} & \frac{97}{10} & \frac{7969}{60} & \frac{2983}{10} & \frac{10597}{60} \\ 0 & 308 & 1814 & 3020 & 1514 \\ -\frac{14}{5} & \frac{558}{5} & \frac{11603}{15} & \frac{7042}{5} & \frac{11239}{15} \\ 0 & 28 & \frac{518}{3} & 292 & \frac{442}{3} \\ -\frac{1}{60} & -\frac{41}{20} & -\frac{977}{120} & -\frac{159}{20} & -\frac{221}{120} \end{pmatrix}, \quad \mathbf{B}^d(5) = \begin{pmatrix} 0 & \frac{45938}{225} & \frac{136048}{75} & \frac{2303461}{450} & \frac{420152}{75} & \frac{941863}{450} \\ 0 & \frac{531083}{450} & \frac{1125787}{100} & \frac{59852027}{1800} & \frac{3846213}{100} & \frac{27519641}{1800} \\ 0 & \frac{33296}{25} & \frac{2777957}{225} & \frac{16131283}{450} & \frac{9199243}{225} & \frac{7223789}{450} \\ 0 & \frac{35314}{75} & \frac{972896}{225} & \frac{2810887}{225} & \frac{3189904}{225} & \frac{1245971}{225} \\ 0 & \frac{13361}{450} & \frac{29329}{100} & \frac{541003}{600} & \frac{314413}{300} & \frac{737947}{1800} \\ 0 & -\frac{3769}{900} & -\frac{19769}{1800} & -\frac{4087}{1200} & -\frac{569}{1800} & -\frac{11063}{3600} \end{pmatrix},$$

$$\mathbf{B}^d(6) = \begin{pmatrix} -\frac{3161}{1500} & \frac{26927833}{108000} & \frac{4598004583}{1512000} & \frac{5795932571}{378000} & \frac{1855393303}{56000} & \frac{24357112027}{756000} & \frac{4396126631}{378000} \\ 0 & \frac{6898699}{1575} & \frac{968634697}{15750} & \frac{8855842207}{31500} & \frac{105342988399}{189000} & \frac{15755047813}{31500} & \frac{31526579237}{189000} \\ -\frac{3703}{300} & \frac{403751777}{108000} & \frac{37990647151}{648000} & \frac{30799301317}{108000} & \frac{47795705483}{81000} & \frac{3286459717}{6000} & \frac{24361535093}{129600} \\ 0 & \frac{297424051}{75600} & \frac{40853120603}{756000} & \frac{3436866121}{14000} & \frac{11464395464}{23625} & \frac{82144827239}{189000} & \frac{36476848183}{252000} \\ -\frac{3179}{1500} & \frac{305626919}{756000} & \frac{1107731089}{181440} & \frac{4560915011}{151200} & \frac{10265293207}{162000} & \frac{7536347671}{126000} & \frac{3794314171}{181440} \\ 0 & \frac{46649}{1575} & \frac{17643341}{47250} & \frac{29754191}{15750} & \frac{364325537}{94500} & \frac{18243773}{5250} & \frac{12233309}{10500} \\ \frac{3}{500} & \frac{5949379}{504000} & \frac{484129979}{9072000} & \frac{2493949}{31500} & \frac{161105327}{9072000} & -\frac{10236563}{504000} & -\frac{2100869}{4536000} \end{pmatrix},$$

$$\mathbf{B}^d(7) = \begin{pmatrix} 0 & \frac{397333711}{236250} & \frac{912481651201}{31752000} & \frac{173427383585083}{952560000} & \frac{799148282837}{1512000} & \frac{183712783847737}{238140000} \\ 0 & \frac{15055932377}{945000} & \frac{19265448332759}{63504000} & \frac{530128616599171}{272160000} & \frac{202315617785353}{35280000} & \frac{8115116669833181}{952560000} \\ 0 & \frac{537797233}{16875} & \frac{57011835834479}{95256000} & \frac{10827125498380181}{2857680000} & \frac{5250459223599319}{476280000} & \frac{11578483272574709}{714420000} \\ 0 & \frac{292847801}{11250} & \frac{93962755567787}{190512000} & \frac{17995590164805689}{5715360000} & \frac{8785533736833223}{952560000} & \frac{974328124477473}{714420000} \\ 0 & \frac{4326178303}{472500} & \frac{8108389258903}{47628000} & \frac{1547327421338977}{1428840000} & \frac{754417201616777}{238140000} & \frac{3344755232825411}{714420000} \\ 0 & \frac{8685673}{7500} & \frac{4079789421839}{19051200} & \frac{793436945079797}{5715360000} & \frac{55667390342629}{136080000} & \frac{107916030493711}{178605000} \\ 0 & \frac{27559079}{945000} & \frac{11827172977}{27216000} & \frac{3547898619617}{1143072000} & \frac{9219646684781}{952560000} & \frac{8647995409723}{571536000} \\ 0 & -\frac{279383}{70000} & -\frac{2224959083}{54432000} & -\frac{162197063431}{11430720000} & -\frac{421769056267}{1905120000} & -\frac{434184850123}{5715360000} \end{pmatrix} \dots \dots$$

$$\begin{pmatrix} \frac{87110688611}{15876000} & \frac{20517348363031}{136080000} \\ \frac{493432968607007}{79380000} & \frac{3373911641427409}{1905120000} \\ \frac{398276643093449}{34020000} & \frac{9436217113175831}{2857680000} \\ \frac{4718411159783921}{476280000} & \frac{3212480565675379}{1143072000} \\ \dots \dots & \frac{1375712097341929}{1428840000} \\ \frac{28904032500311}{8505000} & \frac{1375712097341929}{1428840000} \\ \frac{207224725526201}{476280000} & \frac{99107423249021}{816480000} \\ \frac{338682310657}{29767500} & \frac{18442465574893}{5715360000} \\ \frac{16530496043}{476280000} & -\frac{13030989991}{2286144000} \end{pmatrix},$$

$$\mathbf{B}^d(8) = \left( \begin{array}{ccccc} -\frac{315276383}{64260000} & \frac{2788741300997412661}{972582811200000} & \frac{1367043564877117357}{25261891200000} & \frac{83668627281908448049}{182359277100000} & \frac{33700440149666544069539}{17506490601600000} \\ 0 & \frac{43765104774011}{764032500} & \frac{28024187907003197}{198648450000} & \frac{5389618946891445769}{446959012500} & \frac{1050536592960008240431}{21454032600000} \\ -\frac{3933833861}{80325000} & \frac{17201231547840084109}{1945165622400000} & \frac{817038838348186882951}{353666476800000} & \frac{59977587466719441052789}{2917748433600000} & \frac{1505686264504828318680281}{17506490601600000} \\ 0 & \frac{44419931204714423}{293388480000} & \frac{47827258839539894509}{12713500800000} & \frac{395154853935328437281}{12259447200000} & \frac{13493281265625073581797}{102979356480000} \\ -\frac{9702061}{315000} & \frac{206234437563110213}{4400827200000} & \frac{4033391679143310347}{3269185920000} & \frac{473921127831031617683}{42908065200000} & \frac{2985505579185826448329}{64362097800000} \\ 0 & \frac{2368934530074779}{125737920000} & \frac{7290035098296442379}{16345929600000} & \frac{323411483779967104817}{85816130400000} & \frac{7838859586585197529459}{514896782400000} \\ -\frac{16082767}{11475000} & \frac{592152467309470673}{389033124480000} & \frac{22011497665815279697}{778066248960000} & \frac{12481333639755250253}{56110546800000} & \frac{773891315884646538521}{8753245300800000} \\ 0 & \frac{2272417081}{69457500} & \frac{58682998912897}{108353700000} & \frac{36890627729928373}{7801466400000} & \frac{192505370574765427}{9361759680000} \\ \frac{104597}{91800000} & -\frac{841786729152769}{778066248960000} & -\frac{61448270893941083}{555761606400000} & -\frac{102103272786152767}{364718554200000} & -\frac{729654237448525603}{7002596240640000} \end{array} \right) \cdot \left( \begin{array}{cccc} \frac{6345630203881728810623}{1458874216800000} & \frac{7243061034581239521359}{1346653123200000} & \frac{1438244989106929453141}{4168821204800000} & \frac{15828728653296464701673}{17506490601600000} \\ \frac{152036745896413284299}{1430268840000} & \frac{494165012642414929513}{3900733200000} & \frac{559191738503504103241}{7151344200000} & \frac{838693437524617003943}{42908065200000} \\ \frac{2231401312787071933213}{11670993734400} & \frac{1627676869932832454158343}{7002596240640000} & \frac{15493657916750060626829}{106099943040000} & \frac{129929631322226023742719}{3501298120320000} \\ \frac{488280046911468358531}{1716322608000} & \frac{349005014669841257446871}{1029793564800000} & \frac{5124332464670408241073}{24518894400000} & \frac{5372707806003957287993}{102979356480000} \\ \frac{8875339744294997232979}{85816130400000} & \frac{3709866338378611902617}{29422673280000} & \frac{13634491690726632965003}{171632260800000} & \frac{5212373807745931214239}{257448391200000} \\ \frac{706660785334913765471}{21454032600000} & \frac{3663713001152510819389}{93617596800000} & \frac{4134432225011965193263}{171632260800000} & \frac{281309819466721802633}{46808798400000} \\ \frac{511947365891879033131}{26524985760000} & \frac{11692325950480172454077}{5001854457600000} & \frac{8638140751830018784711}{5835496867200000} & \frac{3363785027662396568069}{8753245300800000} \\ \frac{371686362676910173}{7801466400000} & \frac{671427062862928823}{11702199600000} & \frac{135795626230911767}{3900733200000} & \frac{58422103525040867}{6686971200000} \\ \frac{1302865197722412781}{2917748433600000} & \frac{8600742285944529613}{35012981203200000} & -\frac{19864685154306389}{166728481920000} & \frac{200810348470291303}{35012981203200000} \end{array} \right)$$

## APPENDIX B: SENSITIVITY OF PADÉ RESUMMATION

A key step for us to get the critical hopping amplitude and the corresponding critical exponent  $z\nu$  from our eighth order strong coupling expansion series is using the Padé resummation method as follows:

$$f(t) = \frac{\sum_{n=0}^{n_{\max}} a_n t^n}{1 + \sum_{m=0}^{m_{\max}} b_m t^m}. \quad (\text{B1})$$

The coefficients  $a_n$  and  $b_m$  could be calculated by fitting with the restriction  $n_{\max} + m_{\max} = 8$ . The most natural way to choose the parameters  $(n_{\max}, m_{\max})$  is (4,4). To check the effect of Padé degrees chosen, we compare (4,4) results with the case of (5,3) and (3,5). As shown in Fig. 5, the small discrepancy of both the critical hopping amplitude and critical exponents demonstrates that Padé degrees have less influence.

- 
- [1] M. Greiner, O. Mandel, T. Esslinger, T. W. Hänsch, and I. Bloch, *Nature (London)* **415**, 39 (2002).
  - [2] M. P. A. Fisher, P. B. Weichman, G. Grinstein, and D. S. Fisher, *Phys. Rev. B* **40**, 546 (1989).
  - [3] D. Jaksch, C. Bruder, J. I. Cirac, C. W. Gardiner, and P. Zoller, *Phys. Rev. Lett.* **81**, 3108 (1998).
  - [4] I. Bloch, J. Dalibard, and W. Zwerger, *Rev. Mod. Phys.* **80**, 885 (2008).
  - [5] C. Gross and I. Bloch, *Science* **357**, 995 (2017).
  - [6] S. Sachdev, *Quantum Phase Transitions* (Wiley Online Library, New York, 2007).
  - [7] T. Stöferle, H. Moritz, C. Schori, M. Köhl, and T. Esslinger, *Phys. Rev. Lett.* **92**, 130403 (2004).
  - [8] A. Vogler, R. Labouvie, G. Barontini, S. Eggert, V. Guarnera, and H. Ott, *Phys. Rev. Lett.* **113**, 215301 (2014).
  - [9] N. D. Mermin and H. Wagner, *Phys. Rev. Lett.* **17**, 1133 (1966).
  - [10] T. D. Kühner and H. Monien, *Phys. Rev. B* **58**, R14741 (1998).
  - [11] B. Capogrosso-Sansone, N. V. Prokof'ev, and B. V. Svistunov, *Phys. Rev. B* **75**, 134302 (2007).
  - [12] B. Capogrosso-Sansone, S. G. Söyler, N. Prokof'ev, and B. Svistunov, *Phys. Rev. A* **77**, 015602 (2008).
  - [13] A. F. Ho, M. A. Cazalilla, and T. Giamarchi, *Phys. Rev. Lett.* **92**, 130405 (2004).
  - [14] M. A. Cazalilla, A. F. Ho, and T. Giamarchi, *New J. Phys.* **8**, 158 (2006).
  - [15] C. Bourbonnais and L. G. Caron, *Int. J. Mod. Phys. B* **5**, 1033 (1991).
  - [16] S. Bergkvist, A. Rosengren, R. Saers, E. Lundh, M. Rehn, and A. Kastberg, *Phys. Rev. Lett.* **99**, 110401 (2007).
  - [17] J. S. You, H. Lee, S. Fang, M. A. Cazalilla, and D.-W. Wang, *Phys. Rev. A* **86**, 043612 (2012).
  - [18] J. P. Ronzheimer, M. Schreiber, S. Braun, S. S. Hodgman, S. Langer, I. P. McCulloch, F. Heidrich-Meisner, I. Bloch, and U. Schneider, *Phys. Rev. Lett.* **110**, 205301 (2013).

- [19] J. Schonmeier-Kromer and L. Pollet, *Phys. Rev. A* **89**, 023605 (2014).
- [20] X.-F. Zhang, T. Wang, S. Eggert, and A. Pelster, *Phys. Rev. B* **92**, 014512 (2015).
- [21] B. Irsigler and A. Pelster, *Phys. Rev. A* **95**, 043610 (2017).
- [22] K. B. Efetov and A. I. Larkin, Sov. Phys. JETP **39**, 1129 (1974).
- [23] B. V. Svistunov, *Phys. Rev. B* **54**, 16131 (1996).
- [24] A. Avella and F. Mancini, *Strongly Correlated Systems-Numerical Methods* (Springer-Verlag, Berlin, 2013).
- [25] J. K. Freericks and H. Monien, *Phys. Rev. B* **53**, 2691 (1996).
- [26] A. Eckardt, *Phys. Rev. B* **79**, 195131 (2009).
- [27] T. Wang, X.-F. Zhang, C.-F. Hou, S. Eggert, and A. Pelster, *Phys. Rev. B* **98**, 245107 (2018).
- [28] S. Eggert, in *Theoretical Survey of One Dimensional Wire Systems*, edited by Y. Kuk *et al.* (Sowha, Seoul, 2007), Chap. 2.
- [29] A. Metavitsiadis and S. Eggert, *Phys. Rev. B* **95**, 144415 (2017).
- [30] L. Pollet, N. V. Prokof'ev, and B. V. Svistunov, *Phys. Rev. Lett.* **104**, 245705 (2010).